Study on Electromagnetic-Fluid-Temperature Multiphysics Field Coupling Model for Drum of Mine Cable Winding Truck

Weihua Chen, Mingliang Zhou, Xiaoheng Yan, Zhengxing Li and Xiaoxue Lin

***Abstract*—Aiming at solving problems of low efficiency, low cable capacity in current 300m open-pit mine cable winding truck, a 900 m cable winding plan was proposed. In this paper, the mechanism of the thermal effect of the cable was described, and a two-dimensional axisymmetric electromagnetic-fluid-temperature multiphysics coupling model of the cable reel was established regarding the 900m cable reel as independent system. Considering the structure of the drum, the number of cable winding layers, the factors of heat conduction, heat radiation and convective heat transfer in the actual working process, the steady state analysis of the multi-physical field coupling was carried out. The sum of the losses of each part of the cable was obtained through the calculation of electromagnetic field, which was used as a heat source to calculate and analyze the temperature distribution of different layers of cable winding, as well as the temperature distribution and heat dissipation characteristics of different structures of the drum. The results show that three layers of cable winding is the best design. The lowest temperature of closed cylindrical drum is 70℃ after heat dissipation, which has obvious advantages compared with the lowest temperature of 85℃ after heat dissipation of squirrel-cage cylindrical drum. The results provide a reliable theoretical basis for the research and development of a new type of mine cable winding truck with 900 m cable capacity.**

***Index Terms*—Heat dissipation characteristics, mine cable winding truck, multiphysics coupling, temperature distribution**

I. Introduction

THE main power supply equipment of the open-pit coal mining tool shovel is the plough truck and the cable winding truck. Although the plough truck has been improved for many times, its poor flexibility, small cable capacity and severe cable abrasion seriously affect the working efficiency of the shovel. The advent of cable winding truck greatly improves power supply flexibility and reduces cable wear, but the unwinding cable capacity is still only 300m. The research of the cable winding truck with the capacity of 900 m enables the open-pit coal mine to get rid of the production constraints of the traditional power supply equipment and improves the working efficiency of the shovel. Its internal structure is shown in Fig. 1. Because the new type of cable winding truck carrying cable adopts the cylindrical multi-layer winding mode, it is bound to cause the heat accumulation of the cable, which has become the decisive factor for the stable operation of the cable winding truck. Therefore, it is very important to simulate and analyze the heat source and heat dissipation process during the process of cable winding truck with cable.

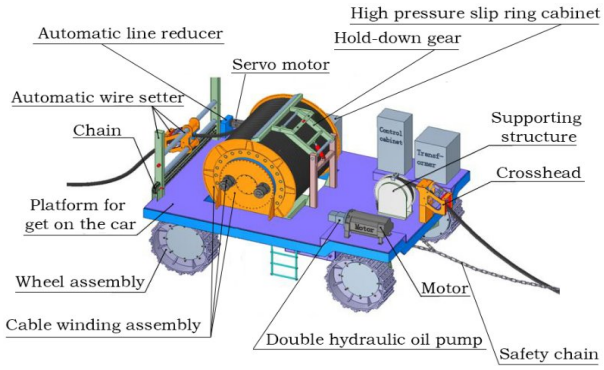

Fig. 1. Cable winding and discharging structure diagram.

At present, scholars at home and abroad have noticed that the temperature rise of cables cannot be ignored under the working conditions of high voltage and high current, and have carried out relevant researches on this issue. In 2015, Ravichandran et al. [1] used the finite element analysis software to study the heat dissipation of a submarine wound cable, and the research results enabled us to understand the heat dissipation of the inner layer of the cable; Trufanova et al. [2] conducted an experimental study on the temperature rise of the cable with high current, and obtained its thermal characteristics curve; Marshall et al. [3] used lumped parameter method to predict the cable temperature field, which made the prediction result close to the real temperature value; In 2016, Lu Anqiang et al. [4] studied the temperature rise characteristics of three-core submarine cables. In 2017, Hao Yanpeng et al. [5] studied the

Manuscript received August 23, 2020; revised November 11, 2020; accepted December 01, 2020. date of publication June 25, 2021; date of current version June 18, 2021.

This work was supported in part by 2019 Local Project of Science and Technology Research Service of Liaoning Provincial Department of Education(LJ2019FL003) ,and by 2019 Science and Technology Research and Innovation Team Project of Liaoning Provincial Department of Education (LT2019007), and by 2020 Youth Science and Technology Talents "Nursery" Projects of Scientific Research of Liaoning Province Education Department(LJ2020QNL019).
(Corresponding author: Zhou Mingliang)

The authors are with the School of Liaoning Technical University (Huludao) , Liaoning Huludao 125100, China(e-mail: fxlgd@163.com; 1793143335@qq.com; xiaohengyan@163.com; 1466686496@qq.com; 1604006222@qq.com)

Digital Object Identifier 10.30941/CESTEMS.2021.00017

influence of the laying and laying methods of submarine high-voltage DC cable on the radial temperature distribution; In 2019, Liang Zhengbo et al. [6] revealed the temperature field distribution characteristics of submarine high-voltage DC cable by calculating the finite element model. Literature [7]-[11] calculated and analyzed the temperature fields of different types of cables under different laying conditions and overload conditions. [12]-[13] studied the cable temperature characteristics under ventilation and explored the influence of air flow on the cable temperature field. Looking at the research status of cable heat production and heat dissipation at home and abroad, most of the research emphases are based on the generation and calculation of cable heat under different linear laying conditions, and the theoretical analyses are relatively sound, but the analyses of cable winding and heat dissipation are very rare. So far, multi-field coupling method has been used to study electromagnetic problems in many fields [14]-[17], but there have been no relevant researches on the temperature rise characteristics and heat dissipation of the cable wound in land air. Beijing university of science and technology Wang Baoying et al. [18] have done about drum winding conductor temperature rise test, the test was found in with about 10 A valid values for current, temperature rose to reach around 30 ℃. From this, it is not difficult to see that when the cable with large current is arranged on the reel with a large number of layers, it is bound to cause a large amount of heat accumulation. Not only will it greatly increase the power loss and shorten the service life of the cable, but also it has great hidden danger to the personal safety of the staff and the safe operation of the equipment. Therefore, it is very important to study the temperature characteristics and heat dissipation characteristics of the multi-layer cable arrangement drum when it is working normally.

In this paper, different winding schemes of 900m cable were proposed for the first time, and the temperature characteristics and heat dissipation characteristics of the multi-layer cable arrangement drum during normal operation were analyzed and calculated. The electromagnetic fluid-temperature multi-physical field coupling model was established by COMSOL software. The finite element analysis method was used to analyze the multiphysics field coupling of the cable and its drum, and then the temperature rise characteristics of the cable with different layers and the heat dissipation characteristics of the drum structure were obtained. It provides a reliable theoretical basis for the research and development of a new type of cable winding with 900 m capacity.

II. THEORETICAL BASIS

To study the electromagnetic-fluid-temperature multi-physical coupling model of cable and drum, the total heat source, namely the total loss, should be defined first. In the process of heating and heat dissipation to equilibrium, the governing equation can be used to describe the process of loading current in the conductor, the flow of air, the heat transfer in fluid and solid, and the electrothermal coupling.

A. Electromagnetic Field Analysis

The governing equation of the electric field module is expressed as equation (1):

$$\begin{cases} \nabla \cdot \boldsymbol{J} = Q_j \\ \boldsymbol{J} = \sigma \boldsymbol{E} + \boldsymbol{J}_e \\ \boldsymbol{E} = -\nabla \varphi \end{cases} \tag{1}$$

Where ∇ is a vector differential operator; $\boldsymbol{J}$ is the current density vector, A/m^3 ; Q_j is the current source, A/m^3 ; σ is the conductivity, S/m; $\boldsymbol{E}$ is the electric field intensity vector, V/m ; φ is electric potential, V ; $\boldsymbol{J}_e$ is the external current density, A/m^3. In this system of equations, the basic parameter of the solution is φ, other parameters are based on it.

The losses calculated for mine high voltage cables include copper conductor current loss, metal sheath loss and dielectric loss of insulating layer.

1) Conductor Loss of Cable Core

According to the international standard IEC 60287, the core loss formula per unit length is expressed as equation (2):

$$\begin{cases} W_c = I^2 R \\ R = r\left(1 + y_s + y_p\right) \end{cases} \tag{2}$$

Where W_c is the resistance loss per unit length of copper conductor of cable, W/m; $\boldsymbol{I}$ is the load current flowing through the copper conductor, **A; R** is the AC resistance per unit length at a given temperature, Ω / m . r is the DC resistance of the conductor core at a given temperature, Ω / m ; y_s is skin effect coefficient; y_p is proximity effect coefficient.

The parameters in equation (2) are calculated as described below:

(a) The DC resistance r per unit length of the cable core can[19] be expressed as equation (3):

$$r = \frac{\rho_{20}}{S}\left[1 + \alpha\left(\theta - 20\right)\right] K_1 K_2 K_3 \tag{3}$$

Where r is the DC resistance per unit length of the cable core at θ℃ , Ω / m ; ρ_{20} is the DC resistance coefficient of the conductor wire core in the condition of 20℃ (copper core ρ_{20} =0.0184×10-6 Ω / m); S is the cross-sectional area of the conductor wire core, m^2 ; α is the resistance temperature coefficient of the conductor (at 20℃, copper α =0.00393℃$^{-1}$); K_1 is the twisting coefficient of wire (Fixed laying cable takes 1.01-1.012; Portable flexible cable takes 1.024-1.05); K_2 is the conductor cabling coefficient (Fixed laying cable takes 1.003-1.012; Portable flexible cable takes 1.030-1.18); K_3 is the compression effect coefficient (Fixed laying cable takes 1.005-1.01).

(b) According to the international standard IEC60287, skin effect coefficient y_s and adjacent effect coefficient y_p of cable are expressed as (4) and (5) respectively:

$$\begin{cases} y_s = \dfrac{x_s^4}{192 + 0.8 x_s^4} \\ x_s^2 = \dfrac{8\pi f}{r} \times 10^{-7} K_s \end{cases} \tag{4}$$

Where f is the AC power supply frequency, Hz; K_s is a constant, determined by the structure of the cable core, it takes 1 here.

$$\begin{cases} y_p = \dfrac{x_p^4}{192+0.8x_p^4}\left(\dfrac{d_c}{s}\right)^2 \times \left[0.312\left(\dfrac{d_c}{s}\right)^2 + \dfrac{1.18}{\dfrac{x_p^4}{192+0.8x_p^4}+0.27}\right] \\ x_p^2 = \dfrac{8\pi f}{R}\times 10^{-7} K_P \end{cases} \tag{5}$$

Where d_c is the outside diameter of the cable core,; s is the distance between the center axes of each cable core, m; K_p is a constant, determined by the core structure of the cable, it takes 0.8 here.

2) Loss Coefficient of Cable Metal Sheath

The metal sheath loss of the cable includes the loss coefficient of the metal shield layer and the loss coefficient of the armor layer. Since the SHD-GC mine cable adopted in this paper has no armor layer, the loss coefficient of the metal shield layer is only analyzed. The cable used in this mine is a three-core cable, each core has a metal shield layer, the calculation formula of metal shielding loss factor is as follows [20]:

$$\begin{cases} \eta_1 = \dfrac{R_s}{R}\dfrac{1.5}{1+\left(\dfrac{R_s}{X}\right)^2} \\ X = 2\omega 10^{-7}\ln\left(\dfrac{2s}{d}\right) \end{cases} \tag{6}$$

Where R_s is the resistance of the metal shield at the working temperature, Ω/m; X is the reactance per unit length of metal shield, Ω/m; d is the average diameter of the metal shield, mm.

3) Cable Dielectric Loss

Dielectric loss of cable [21] refers to the energy loss of insulating material of cable caused by dielectric conductance and hysteresis effect under the action of alternating voltage. The insulation loss per phase unit length of the cable is expressed as equation (7):

$$\begin{cases} W_d = \omega c U_0^2 \tan\delta \\ c = \dfrac{\varepsilon}{18\ln\dfrac{D_i}{d_c}}\times 10^{-9} \end{cases} \tag{7}$$

Where $\omega = 2\pi f$,f=50 Hz; c is the capacitance per unit length of cable, $\mathrm{F/m}$; U_0 is the cable voltage to the ground (Namely phase voltage),V; $tan\delta$ is the insulation loss factor. In the case of operating temperature and power frequency current, it is generally 0.004. ε is the dielectric constant of the insulating material ,which takes 2.3 $\mathrm{F/m}$. D_i is insulation layer diameter (except shielding layer), mm; d_c is the conductor diameter (including the shield if any), mm.

As the field space of the electromagnetic field inside the cable is composed of a variety of media, the boundary conditions of the interface between different media regions should be introduced into the basic partial differential equation, it can be described as equation(8):

$$\begin{cases} \Omega : \dfrac{1}{\mu}\dfrac{\partial^2 \boldsymbol{A}}{\partial r^2} + \dfrac{1}{\mu\rho^2}\dfrac{\partial^2 \boldsymbol{A}}{\partial r^2} = -\boldsymbol{J} \\ \Omega^1 : \boldsymbol{J} = -\dfrac{1}{\rho(T)}\left(\nabla\phi + \dfrac{\partial A}{\partial t}\right) \\ \Omega^2 : \boldsymbol{J} = 0 \\ C : A_1 = A_2 \\ C : \dfrac{1}{\mu_1}\dfrac{\partial \boldsymbol{A}_1}{\partial n} = \dfrac{1}{\mu_2}\dfrac{\partial \boldsymbol{A}_2}{\partial n} \\ \Gamma : \boldsymbol{A} = 0 \end{cases} \tag{8}$$

Where Ω is the whole electromagnetic field solution area; Ω^1 is the conductor area; Ω^2 is the air area; C is the boundary between different media; Γ is outer boundary of air; $\boldsymbol{J}$ is the current density, $\mathrm{A/m^2}$; μ is the permeability of the medium, $\mathrm{H/m}$; μ_1、μ_2 are the permeability of two different media regions, $\mathrm{H/m}$. $\boldsymbol{A}$ is the vector magnetic potential of the electromagnetic field solution region, $\mathrm{Wb/m}$; $\boldsymbol{A}_1$、$\boldsymbol{A}_2$ are the vector magnetic potential at the boundary of different electromagnetic field solution regions, $\mathrm{Wb/m}$; ρ is the resistivity of materials related to conductor temperature, Ω/m; T is conductor temperature, ℃; ϕ is a scalar potential, V. $\nabla\phi$ is unknown in equation (2), no unique solution to it, thus gives the definite condition in (4). In the second equation $\nabla\phi$ is unknown, and there is no unique solution for the equation. Therefore, the conditions for determining the solution are given as follows (9).

$$\iint_\Omega \boldsymbol{J} ds = \boldsymbol{I} \tag{9}$$

Where Ω is the whole electromagnetic field solution area; J is the current density, $\mathrm{A/m^2}$; $\boldsymbol{I}$ is the total current flowing through the cable core section, A.

B. Thermal Fluid Field Analysis

The temperature field in the solid should satisfy the law of energy conservation and fourier law. Based on the assumption of the constant physical property of the object, the solution of the steady-state temperature field in the cable calculation area can be reduced to the following boundary value problem [22],[23].

$$\begin{cases} \Omega : \lambda\dfrac{\partial^2 T}{\partial r^2} + \dfrac{\lambda}{r^2}\dfrac{\partial^2 T}{\partial \theta^2} + Q_\upsilon = 0 \\ L : -\lambda\dfrac{\partial T}{\partial n} = -\lambda^*\dfrac{\partial T^*}{\partial n} + \sigma_0\varepsilon\left(T - T^*\right) \\ L : T = T^* \\ C : T_1 = T_2 \\ C : \lambda_1\dfrac{\partial T_1}{\partial n} = \lambda_2\dfrac{\partial T_2}{\partial n} \end{cases} \tag{10}$$

Where Ω is the conductor temperature field solution area; L is the boundary between the wire and the surrounding air region; C is the boundary between two solid solution regions; T is the temperature of solid material, ℃; λ is the thermal conductivity of solid material, $\mathrm{W/(m\cdot K)}$; Q_V is the heat yield per unit volume of each layer conductor, $\mathrm{W/m^3}$; λ^* is the thermal conductivity of the air, $\mathrm{W/(m\cdot K)}$; T^* is the air temperature, which can be solved by the fluid domain, ℃; σ_0 is Stephen-Boltzmann constant of $5.67\times10^{-8}\left(\mathrm{m^2\cdot K^4}\right)$; ε is the surface emissivity of wire, and the new bright line is 0.23~0.46, T_1 and T_2 are the temperature on both sides of the solid boundary, ℃.

The governing equation of flow field module is expressed as (11)[24]:

$$\begin{cases} \nabla\cdot(\rho_1\boldsymbol{v})=0 \\ \rho_1(\boldsymbol{v}\cdot\nabla)v=-\nabla p+\nabla\cdot\left(\mu\left(\nabla\boldsymbol{v}+(\nabla\boldsymbol{v})^T\right)-\frac{2}{3}\mu(\nabla\boldsymbol{v})I\right) \end{cases} \tag{11}$$

Where ρ_1 is the density of fluid material, $\mathrm{kg/m^3}$; $\boldsymbol{v}$ is the velocity vector, $\mathrm{m/s}$; p is pressure, Pa; μ is dynamic viscosity, $\mathrm{Pa\cdot s}$; I is the identity matrix.

In the calculation of the thermal-flow coupling field of cables and reels, the factors of heat conduction, heat radiation, and convective heat transfer are also taken into account. Heat conduction is the heat transfer phenomenon in the absence of macroscopic motion in the medium, which can occur in solid, liquid and gas. Its governing equation [25],[26] is expressed as (12):

$$\rho C_v\frac{\partial T}{\partial t}=\lambda\left(\frac{\partial^2T}{\partial^2x}+\frac{\partial^2T}{\partial^2y}+\frac{\partial^2T}{\partial^2z}\right)+Q_v \tag{12}$$

Where T is temperature, K; *x, y* and *z* are the coordinates, m; C_v is specific heat capacity, $\left(\mathrm{J\cdot kg^{-1}\cdot K^{-1}}\right)$; ρ is density, $\mathrm{kg/m^3}$; *t* is time, s; Q_v is the heating power per unit volume, $\mathrm{W/m^3}$.

In general, the heat dissipation of cable reels is mainly affected by air flow, and the momentum characteristics of air flow can be studied through calculating fluid dynamics analysis. By solving three conservation equations [27]-[29] simultaneously, the mechanism of convective heat transfer and temperature distribution around the cable drum is predicted.

Continuity equation can be expressed as (13):

$$\nabla\cdot\rho\boldsymbol{v}=0 \tag{13}$$

Momentum conservation equation can be expressed as (14):

$$\rho\frac{\partial\boldsymbol{v}}{\partial t}=\rho\boldsymbol{g}-\nabla p+\xi\nabla^2\boldsymbol{v} \tag{14}$$

Energy conservation equation can be expressed as (15):

$$\rho c_v\frac{\partial T}{\partial t}=\frac{\partial Q}{\partial t}+\nabla^2(kT)+\Phi \tag{15}$$

Where ρ is density, $\boldsymbol{v}$ is velocity vector, $\boldsymbol{g}$ is the acceleration of gravity, ξ is dynamic viscosity, c_v is specific heat capacity, p is pressure, Φ is loss equation.

Since the convection heat transfer coefficient of the external air to the cable drum cannot be directly measured, this paper calculates the heat transfer coefficient according to the experimental correlation formula [30] adopted in engineering:

$$Nu=C(Gr\cdot Pr)^n \tag{16}$$

$$Gr=\frac{g\alpha_v\Delta Tl^3}{v^2} \tag{17}$$

$$Pr=\frac{c_v\xi}{\boldsymbol{\lambda}} \tag{18}$$

$$h=\frac{\boldsymbol{\lambda}}{l}Nu \tag{19}$$

Where α_v is the volume expansion coefficient of the fluid, l is the characteristic length, and ΔT is the temperature difference between the barrel surface and the environment.

Any object whose temperature is above absolute zero is constantly radiating heat outward and absorbing radiation thrown onto its surface by surrounding objects. The radiation power of the actual object can be expressed as (20) [31],[32]:

$$P_f=\varepsilon\sigma_0\left(\frac{T}{100}\right)^4 \tag{20}$$

Where ε is the emissivity of the object; T is the temperature of the object, K

The heat generated by the cable is related to the resistivity of the cable's metal core, which varies with the temperature of the conductor. $\rho(T)=\rho_0\left[1+a(T-T_0)\right]$, Where a is the temperature coefficient of copper, and in this paper, a=0.004

In the model, the heat source is the total loss generated by the current-carrying current in the cable, therefore, the governing equation of the electrothermal coupling module is expressed as (21):

$$\rho C_v\frac{\partial T}{\partial t}+\rho C_v v\cdot\nabla T=\nabla\cdot(\lambda\nabla T)+Q=\nabla\cdot(\lambda\nabla T)-\boldsymbol{J}\cdot\boldsymbol{E} \tag{21}$$

Where ρ is the density of the material; Q is the heat source in the material.

III. Model

A. Physical Model

In this paper, SHD-GC mine cable is adopted. Its geometric structure parameters are shown in Table 1, so as to establish the cable model as shown in Figure 2 in COMSOL.

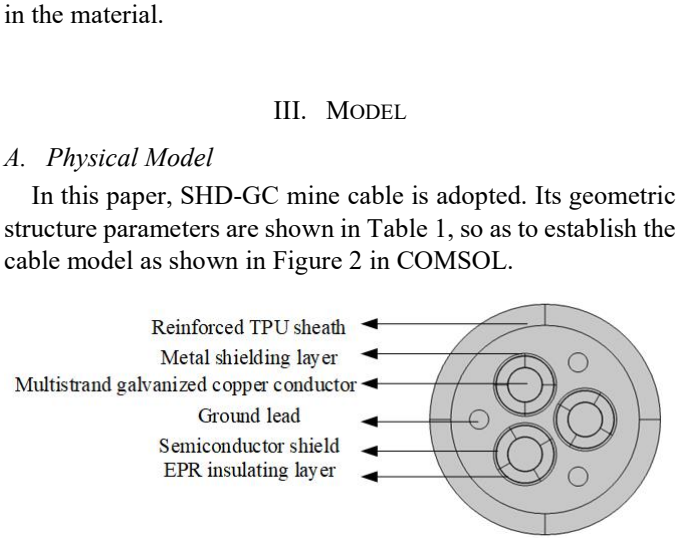

Fig. 2. SHD-GC cable model.

TABLE I
CABLE GEOMETRY PARAMETERS TABLE

Materials	Radius (mm)	Thickness (mm)
Reinforced TPU sheath	35	6.4
Conductive copper	4.72	4.72
PPE insulation	8.4	3.4
Metal shielding layer	9.1	0.7
Detection copper wire	2.83	2.83
Semiconductor mixture 1	4.86	0.14
Semiconductor mixture 2	8.26	0.14

The cable and drum will be placed in the body of the cable winding truck with the size of 7000×5000×3400 mm, and the air field of the flow field between the cable, drum and box, the solution domain of the box and the cable winding of the drum will be established. The solution model is shown in Fig. 3.

In the process of analysis, the number of layers and the structure of the reel were studied. (Considering the mechanical strength of the reel, a high metal alloy steel with thermal conductivity of 120 $\omega/\mathrm{m}\cdot\mathrm{k}$ was selected.) For this reason, the 2-5 layer cable winding scheme and two different drum structures were proposed for comparison. The size of the drum is shown in Table 2, and the structure of the drum is shown in Fig. 4.

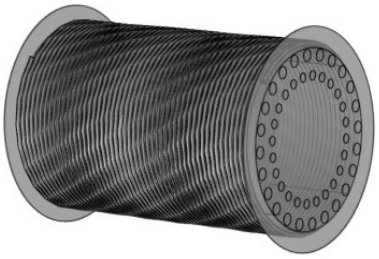

(a)

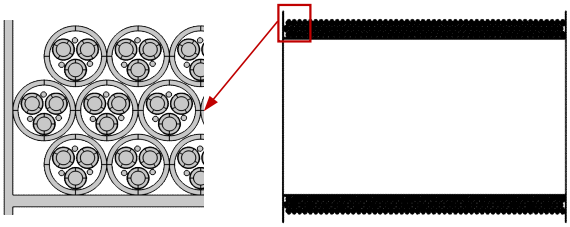

(b)

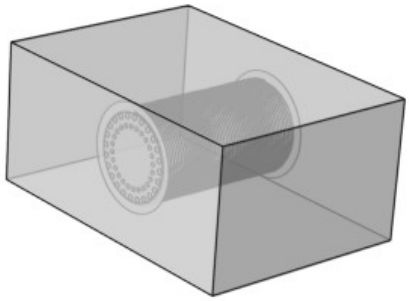

(c)

Fig. 3. Schematic diagram of solution model. (a) Physical model of cable reel wound. (b) Cable and reel model cross section. (c) Schematic diagram of solution domain.

TABLE II
CABLE WINDING SCHEME

Number of layers	2	3	4	5
Drum bottom radius (mm)	1570	1180	1240	1300
Drum cylinder radius (mm)	1420	980	980	980
Drum length (mm)	3555	3415	2715	2085
Reel wall thickness (mm)	10	10	10	10
Cable length (m)	932	970	1060	1034

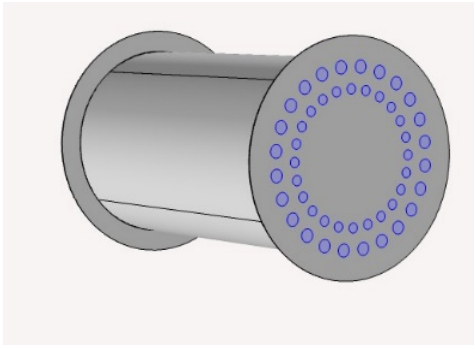

(a)

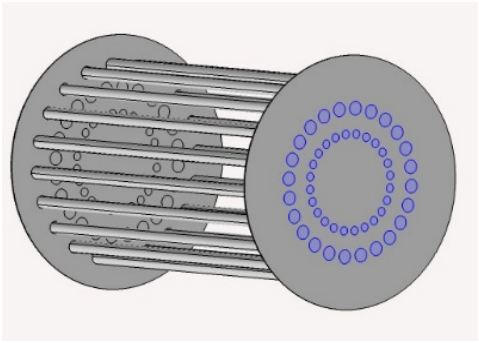

(b)

Fig. 4. Cable drum structure diagram. (a) Enclosed cylindrical drum. (b) Squirrel cage cylindrical drum.

The blue area in Fig. 4 is the vent for the purpose of adding forced convection in the flow field when the temperature is too high.

B. Simulation Model

The following assumptions should be made in the research process:

1) Fluid is considered as a viscous incompressible fluid, and the fluid Mach number Ma<0.3;

2) Fluid temperature is regarded as a constant value, that is, $T = const$;

3) The convection and radiation heat dissipation of the air gap inside the cable is ignored, that is, the air gap only has heat conduction effect;

4) The contact thermal resistance is ignored, that is, R=0;

5) Since the power supply voltage is power frequency, the displacement current and its influence can be ignored;

6) As SHD-GC cable is adopted, the inner cable core is composed of fine copper wire, so skin effect and proximity effect can be ignored.

Three physical interfaces need to be added to the simulation model:

1) Electric field: According to the actual voltage demand of mining tools in open pit coal mines, the frequency is set to 50 Hz , and the effective value of 150 AC current is applied to the three conductor cores of the cable, the details are expressed as (22):

$$\begin{cases} I_a = I_0 \\ I_b = I_0 e^{-j2\pi/3} \\ I_c = I_0 e^{+j2\pi/3} \end{cases} \tag{22}$$

Where I_0 is the effective value of current, and its value is 150 A . Under normal circumstances, the cable copper belt shielding layer is grounded, potential of 0 V.

2) Flow field and heat transfer module: The principles of flow field [33] and heat transfer module [34]-[35] are relatively complex, and the setting is relatively complex. The references in this paper are introduced in clear detail, which will not be repeated in this paper. In the calculation of electric-thermal coupling, the convection heat transfer coefficient between the cable and the air is set at 6.2 $W/\left(m^2 \cdot K\right)$, and the air temperature is 20℃.

IV. Simulation Analysis

In this paper, a two-dimensional axisymmetric electromagneti c- fluid-temperature multiphysics field coupling model for cabl e winding was established according to the actual situation of c able winding in mine cable winding. Considering radiation hea t dissipation, conduction heat dissipation, and natural convecti on heat dissipation factors, simulation calculation and analysis are carried out for different reel structures and different layers of unwinding cable. The material parameters are shown in tabl e 3.

TABLE III
Material Parameters of Each Layer of Cable

Materials	PPE	Semiconductor mixture	Reinforced TPU sheath
Electrical conductivity [s/m]	1e-18	2	1e-18
Relative dielectric constant	2.25	2.25	7
Relative permeability	1	1	1
Thermal conductivity coefficient [w/(m·k)]	0.46	10	0.46
Density[kg/m3]	935	1055	930
Constant pressure heat capacity [J/(kg·k)]	2302	2405	2302

A. Analysis of Electromagnetic Field Simulation Results

The heat source of cable winding and drum comes from the loss of copper conductor, the loss of metal shielding layer and the loss of medium, and the loss of metal shielding layer varies with the change of magnetic field. Therefore, the influence of magnetic field on the loss of metal shielding layer is considered in the research process. COMSOL is used to calculate and analyze the axial magnetic field distribution of a single cable and the magnetic field distribution results of multi-layer cables on the reel (taking three layers as an example), as shown in Fig. 5:

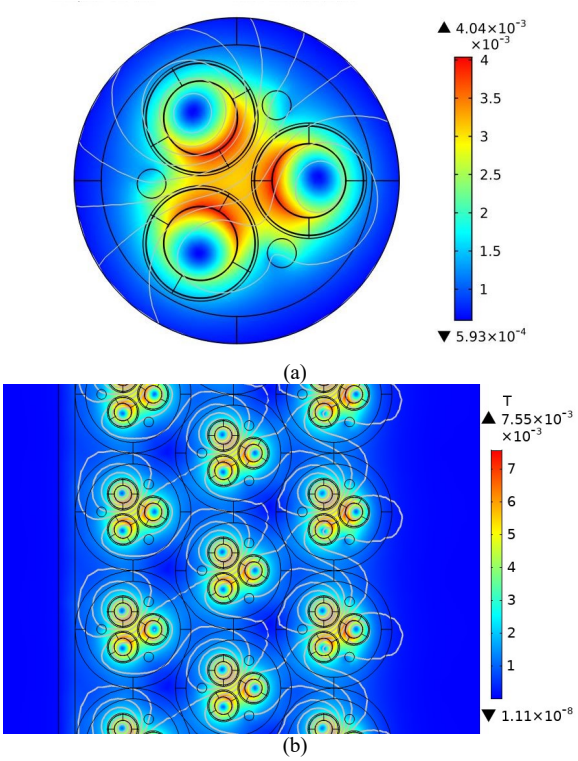

Fig. 5. Distribution of magnetic induction intensity of cable. (a) Distribution diagram of radial magnetic induction intensity of cable. (b) Local distribution diagram of magnetic induction intensity of multi-layer cable in reel

According to the simulation results in Figure 5 (a), it can be clearly seen that the radial magnetic induction line of a single cable gradually weakens outward from the cable core, denser in the cable core, the strength of the magnetic field is weakened because the magnetic fields cancel each other in the center of the three cores caused by the three-phase alternating current, and the magnetic fields of adjacent cables will influence each other when the multi-layer cables are arranged, as shown in Figure 5 (b). It can be observed from the magnetic induction line that the magnetic fields of adjacent cables influence each other, changing the direction of the magnetic induction line and thus the direction of the magnetic field, and at the same time, when the multi-layer cables are arranged on the drum, the magnetic field strength changes from the original maximum value of 4.04×10^{-3} T for a single cable to the maximum value of 7.55×10^{-3} T, and the cable magnetic field strength is significantly enhanced. Therefore, when multi-layer cables are laid on the drum, the loss of metal shielding layer is larger than that of single cable.

Cable loss distribution is shown in Fig. 6.

It can be seen from the figure that the cable losses are mainly concentrated in the three copper conductor, but the losses of the rest parts are not obvious. In order to better observe the other losses, the copper conductor is removed from the solution, and the other losses are shown in Fig. 7.

After removing the loss of copper conductor of cable, the loss of metal shielding layer can be clearly observed, but the value is far less than that of copper conductor, and the loss of insulation layer can be ignored. Therefore, the heat source of mine cable unwinding truck and drum is mainly from the loss of copper conductor and metal shielding layer.

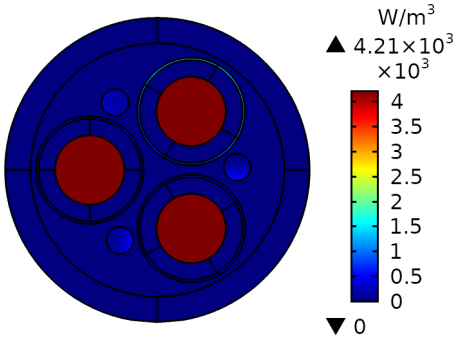

Fig. 6. Internal loss distribution of cable.

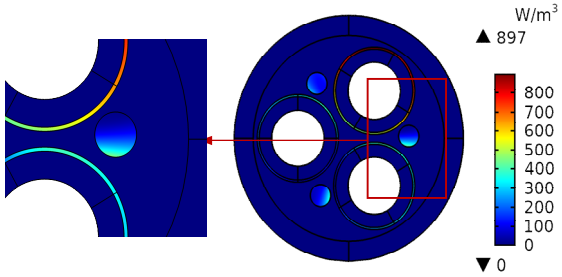

Fig.7. Local loss distribution.

B. *Analysis of Temperature Field Simulation Results*

In the two-dimensional axisymmetric fluid-temperature field analysis of cable and drum, the temperature of 2-5 layers of cable is calculated according to the research scheme, and the temperature distribution of cable and drum is shown in Figure 8:

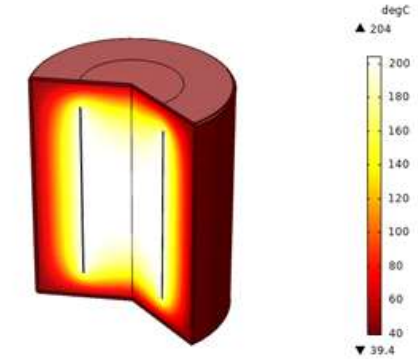

(a)

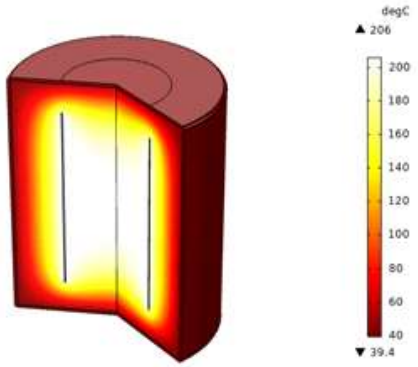

(b)

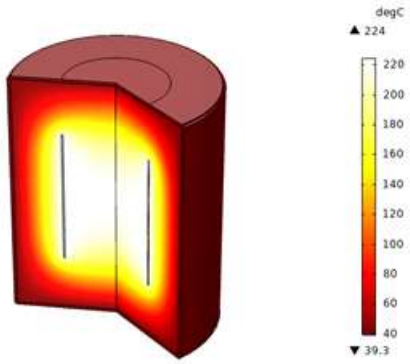

(c)

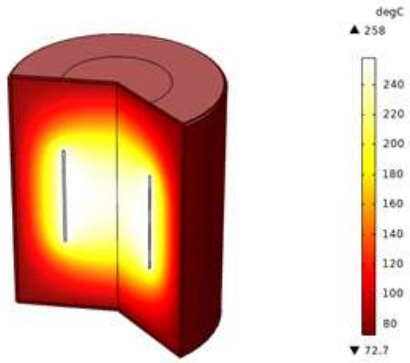

(d)

Fig. 8. Simulation results of temperature rise of multi-layer cable arranged by drum. (a) Two layers temperature simulation results. (b) Three layers temperature simulation results. (c) Four layers temperature simulation results. (d) Five layers temperature simulation results.

It can be seen from the temperature distribution results that, with the cable as the heat source, the temperature gradually decreases in all directions. The temperature on the outside of the cable and the drum model decreases rapidly, whereas the temperature on the inside is much less effective than that on the outside. The main influencing factors are the size of the heat dissipation area and the flow velocity of the air inside and outside the model. The area of heat dissipation on the outside is significantly larger than that on the inside, and the air flow is accelerated when heated, whereas the air flow on the inside is limited by the semi-closed structure of the drum, so that the effect of heat dissipation on the inside is far less than that on the outside. The temperature rise will increase the cable loss and further increase the temperature until it reaches steady state, forming the temperature distribution is shown in Figure 7.In the process of studying the influence of different layers on the temperature distribution, it is necessary to analyze the axial temperature change of the model. Firstly, the following points are taken for the axial direction of the model: a temperature distribution of the geometric center A as the origin, straight to the right is the X-axis, backwards is the Y-axis, and upwards is the z-axis, establish space rectangular coordinate system, straight to the right in turn, take the B(500，0，0), C（970，0，0）, D （1050,0,0）, E (1136,0,0), F (1292，0，0), G (1450,0,0), based on results of calculating the COMSOL, collect each point temperature, the temperature change is shown in Fig. 9:

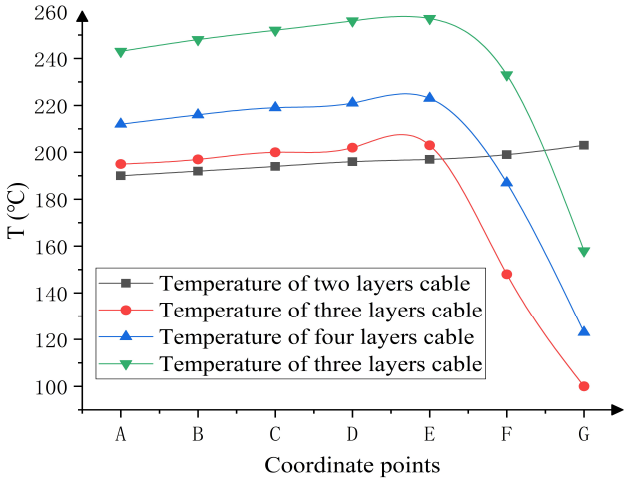

Fig. 9. Temperature change of layer 2-5 winding cable.

It can be seen from Fig. 9 that when the cable temperature reaches steady-state, the temperature change curve of 2-5 layers was compared, and it is found that the temperature increases faster with the increase of layers. Table 2 shows the cable unwinding scheme and the design data of reel size. Due to the large radius of the reel of the two-layer cable, the temperature point is located inside the reel, above the reel and above the cable. Since the heat of the model comes from the cable, the temperature rises from the center of the drum to the cable. While the temperature of the 3-5 layer cable from the center of the drum to the cable increases continuously. When it reaches the outer surface of the cable and the model, the temperature appears an inflection point and drops sharply. The more layers of cable, the higher the temperature. Considering the limitation of the carriage size to the size of the reel, the results of temperature comparison show that the three-layer cable winding is the best design.

C. Analysis of Heat Dissipation of Different Drum Structures

Taking the three-layer cable unrolled by a drum as an example and considering conduction, radiation and natural convection heat dissipation factors, the influence of two different structures designed in this paper on temperature is explored. The temperature simulation results are shown in Fig. 10.

From Fig. 10 you can see, the maximum temperature of enclosed cylindrical drum with cable is 216℃, and that of squirrel cage cylindrical drum with cable is 223℃, the two

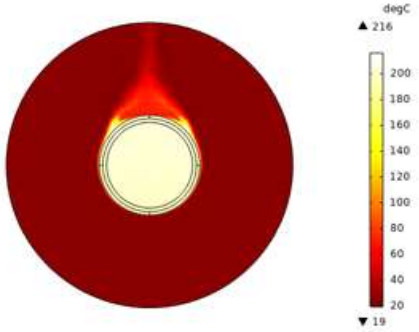

(a)

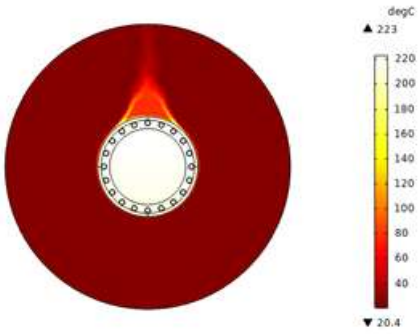

(b)

Fig. 10. The simulation results of the two structures. (a) Enclosed cylindrical drum cable temperature rise. (b)Squirrel-cage cylindrical drum cable temperature rise.

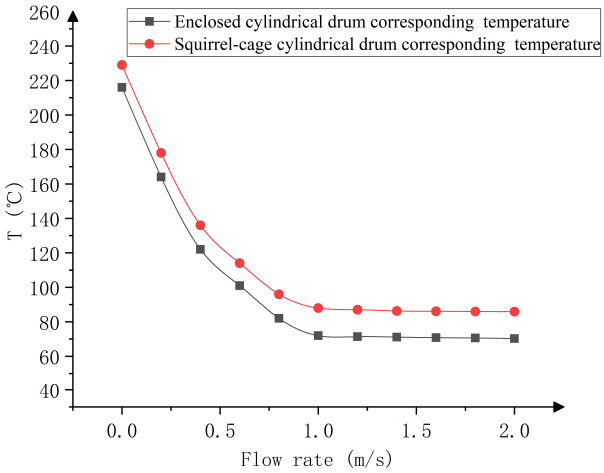

Fig. 11. Cooling characteristic curves of two different structures.

kinds of structures are severe over the cable temperature, apparently only consider conduction, radiation, and natural convection factors do not get two different structures of the cooling characteristic of drum, therefore, COMSOL is used to change the air flow velocity inside the drum and calculate the heat dissipation characteristics of the two structures , as shown in Fig. 11.

It can be seen from Fig. 11 that the cooling effect of these two curves is very significant when the flow velocity is from 0 to 1m/s. The closer the air velocity is to 1m/s, the slower the temperature drops. When the air velocity is closer to 1m/s, the heat dissipation effect is close to saturation. Therefore, when the air velocity is more than 1m/s, the temperature almost stops dropping. Therefore, the optimal cooling wind speed of the two structures is 1m/s.When saturated, the temperature of enclosed cylindrical drum has been reduced from 216℃ to 70℃, and the squirrel-cage cylindrical drum has been reduced from 223℃ to 80℃. Therefore, the heat dispersing characteristics of the enclosed cylindrical drum is better than that of the squirrel-cage cylindrical drum.

V. CONCLUSIONS

In this paper, the electromagnetic- fluid-temperature multiphysics field coupling model of the drum and cable was established. The COMSOL software was used to conduct theoretical analysis and calculation of its physical field by using

the finite element analysis method, and the results were analyzed to draw the following conclusions:

(1) A two-dimensional axisymmetric model of the electroma gnetic-fluid-temperature of the cable and the drum was establis hed. Considering that the electromagnetic properties of the mat erial would change with the temperature, the cable losses were calculated, and the distribution characteristics of the losses wer e mainly concentrated on the conductive copper core and a sma ll amount existed on the metal shield.

(2) The temperature distribution during the 2-5 layers of unwinding cable was calculated respectively. At the same time, the temperature gradient increased with each additional layer of unwinding cable. Considering the internal space of cable unwinding truck, the optimal scheme of cable unwinding was determined to be 3 layers.

(3) In this paper, the heat dissipation effect of two different cable drum structures was calculated, and the heat dissipation characteristic curve was obtained. Through comparative analysis, it is determined that the enclosed cylindrical drum is the best structure of the cable.

REFERENCES

[1] R. Ravichandran, A. Umapathy, S. M. Babu, et al. "Heat dissipation studies on sub-sea cables wound on winches//2015 IEEE Underwater Technology (UT)," *IEEE*, pp. 1-4, 2015.

[2] N. M. Trufanova, E. Y. Navalikhina, T. V. "Gataulin. Mathematical modeling of nonstationary processes of heat and mass transfer in a rectangular cable channel," *Russian Electrical Engineering*, vol. 86, no. 11, pp. 656-660, 2015.

[3] J. S. Marshall, A. P. Fuhrmann. "Effect of Rainfall Events On The Thermal And Moisture Exposure Of Underground Electric Cables," *International Journal of Heat and Mass Transfer*, vol. 80, pp. 660-672, 2015.

[4] A. Q. Lv, X. Kou, C. Q. Yin, et al. "Modeling of temperature relationship between composite optical fiber and conductor in three-core submarine cable," *Transactions of China Electrotechnical Society*, vol. 31, no. 18, pp. 59-65, 2016.

[5] Y. P. Hao, Y. Chen, L. Yang, et al. "Simulation of electric-thermal-current multi-physical field coupling of high voltage DC submarine cable," *High Voltage Engineering*, vol. 43, no. 11, pp. 3534-3542, 2017.

[6] Z. B. Liang, M. Z. Xu, F. Chen, et al. "Thermal characteristics of EHV submarine cable in typical laying environment," *High Voltage Engineering*, vol. 45, no. 11, pp. 3452-3458, 2019.

[7] Y. J. Zhang, Z. L. Wang, B. Z. Xu, et al. "Study on adaptive time step in transient electromagnetic-temperature field coupling calculation," *Transactions of China Electrotechnical Society*, vol. 33, no. 19, pp. 4468-4475, 2018.

[8] H. Wang, X. B. Li, J. H. Lu, etc. "Thermal circuit model modeling of optical fiber composite low voltage cable based on superposition principle," *Transactions of China Electrotechnical Society*, vol. 34, no. 07, pp. 1381-1391, 2019.

[9] X. X. Zhou, Y. K. Jiang, S. H. Wang, et al. "Analysis of influencing factors of long-term temperature rise of directly buried cable," *High Voltage Apparatus*, vol. 53, no. 10, pp. 178-182, 2017.

[10] L. Ruan, A. X. Zhao, D. Deng, et al. "Effect of unbalanced current of three-core cable on temperature distribution," *High Voltage Engineering*, vol. 444, no. 08, pp. 2704-2709, 2018.

[11] K. Liu, Q. Y. Xie. "Evolution characteristics of internal and external temperature field of high voltage cable under overload condition," *Chinese Journal of Safety Science*, vol. 28, no. 1, pp. 92-97, 2018.

[12] L. Exizidis, F. Vallée, Z. De Grève, et al. "Thermal behavior of power cables in offshore wind sites considering wind speed uncertainty," *Applied Thermal Engineering*, vol. 91, pp. 471-478, 2015.

[13] J. Wang, X. Liu, S. Chen, et al. "Reduced-scale model study on cable heat dissipation and airflow distribution of power cabins," *Applied Thermal Engineering*, vol. 160, pp. 114068, 2019.

[14] X. M. Liu, J. X. Xue, Y. M. Yang, et al. "Study on magneto-thermal equivalence and temperature rise in lap joint area of transformer core," *Chinese Journal of Scientific Instrument*, vol. 41, no. 06, pp. 187-196, 2020.

[15] Q. Q. Wang, R. F. Liu, X. J. Ren. "Discharge breakdown of motor bearing based on multi-physical field analysis," *Transactions of China Electrotechnical Society*, vol. 35, no. 20, pp. 4251-4257, 2020.

[16] X. F. Wang, Y. Dai, J. Luo. "Water channel design and temperature field analysis of vehicle permanent magnet synchronous motor based on fluid-solid coupling," *Transactions of China Electrotechnical Society*,vol. 34, no. S1, pp. 22-29, 2019.

[17] C. Pan, X. Chen, G. W. Cai, et al. "Mode-state characteristics of three-phase unbalanced operation winding vibration of transformer based on electromagnetic mechanical coupling principle," *Proceedings of the CSEE*, vol. 40, no. 14, pp. 4695-4707+4747, 2020.

[18] B. Y. Wang, L. Q. Gao, S. B. Liu. "Simulation calculation of temperature rise of fixed multi-layer cable fixed on the reel," *Metal Mine*, vol. 04, pp. 25-29, 1989.

[19] F. S. Zhao. "Mine cable," *Beijing: Coal Industry Press*,1987.

[20] G. D. Ma. "Wire and cable ampacity (2nd edition)," *China Electric Power Press*, 2013.

[21] Y. C. Liang. "Numerical calculation of current carrying capacity of high-voltage power cables," *National Defense Industry Press*, 2012.

[22] W. S. Tao. "Heat transfer," *Xi'an: northwest University of Technology Press*, 2006.

[23] Q. Y. Yin, W. L. Li, H. T. Yu, et al. "Calculation and analysis of electromagnetic field and temperature field in the case of broken strand fault of large synchronous generator," *Transactions of China Electrotechnical Society*, vol. 26, no. 2, pp. 59-67, 2011.

[24] Z. M. Huang, M. L. Fu, Y. P. Hao, et al. "Three-dimensional simulation of temperature control water tank for thermal cycle test of high-voltage DC cables," *Chinese Journal of Electrical Engineering*, vol. 36, no. 11, pp. 3133-3140, 2016.

[25] Y. Zhang, J. Ruan, T. Huang,et al. "Calculation of temperature rise in air-cooled induction motors through 3-D coupled electromagnetic fluid-dynamical and thermal finite-element analysis," *IEEE Transactions on Magnetics*, vol. 48, no. 2, pp. 1047-1050, 2012.

[26] M. B. Eteiba,M. M. Abdel Aziz,J. H. Shazly ."Heat conduction problems in SF6 gas cooled-insulated power transformers solved by the finite-element method," *IEEE Transactions on Power Delivery*,vol.23, no. 3, pp. 1457-1463, 2008.

[27] F. M. White. "Fluid Mechanics", *McGraw-Hill,* 2007.

[28] C. Ortiz, A. W. Skorek, M. Lavoie, et al. "Parallel CFD analysis of conjugate heat transfer in a dry-type transformer," *IEEE Transactions on Industry Applications*, vol. 45, no. 4, pp. 1530-1534, 2009.

[29] S. H. Lee, B. Y. Lee, H. K. Kim, et al. "Local heat source approximation technique for predicting temperature rise in power capacitors," *IEEE Transactions on Magnetics*, vol. 45, no. 3, pp. 1250-1253, 2009.

[30] M. E. Rosillo, C. A. Herrera, G. Jaramillo. "Advanced thermal modeling and experimental performance of oil distribution transformers," *IEEE Transactions on Power Delivery*, vol. 27, no. 4, pp. 1710-1717, 2012.

[31] S. Purushothaman,F. De Leon. "Heat-transfer model for toroidal transformers," *IEEE Transactions on Power Delivery,*2012， 27(2): 813-820.

[32] A. Lefevre,L. Miegeville,J. Fouladgar,et al. "3-D computation of transformers overheating under nonlinear loads," *IEEE Transactions on Magnetics*, vol. 41, no. 5, pp. 1564-1567, 2005.

[33] Z.S. Zhang, G.X. Cui. "Hydromechanics", Tsinghua University Press, 2015.

[34] R.B. Su, P.Wang, G. Liu, et al. "Analysis of Heat Transfer Process and the Finite Element Model of the 10kV Three-Core Pipe Cables," *Advanced Materials Research*, vol. 1008*,* pp. 583-587*,* 2014.

[35] W.X. Li, R. B. Su, G. Liu, et al. "Study on the Steady State Thermal Circuit Model of 10kV Three-Core Cable Based on the Shape Factor Method," *Advanced Materials Research*, vol. 1008*,* pp. 593-597*,* 2014.

Weihua Chen received his B. Sc. degree, M. Sc. degree and Ph. D. degree all from Liaoning Technical University in 2002, 2006 and 2016, respectively. He is currently an associate professor at Liaoning Technical University. His main research interests include the radio energy transmission technology and research on key technologies of mine electromechanical equipment.

Mingliang Zhou received his B. Sc. degree from Liaoning Technical University in 2018. He is currently a M. Sc. candidate at Liaoning Technical University. His main research interest includes intelligent control and electromagnetic coupling.

Xiaoheng Yan received her B. Sc. Degree, M. Sc. degree and Ph. D. degree all from Liaoning Technical University in 2005, 2008, and 2016, respectively. She is currently an associate professor at Liaoning Technical University. Her main research interests include radio energy transmission and electromagnetic detection and imaging.

Zhengxing Li received his B. Sc. degree from Liaoning Technical University in 2019. He is currently a M. Sc. candidate at Liaoning Technical University. His main research interest includes electromagnetic detection and imaging.

Xiaoxue Lin received her B. Sc. degree from Liaoning Technical University in 2019. She is currently a M. Sc. candidate at Liaoning Technical University. Her main research interest includes magnetoacoustic imaging.